Precise and Label-free Tumour Cell Recognition Based on A Black Phosphorus Nanoquenching Platform

Wujuan Yan[a], Xiu-Hong Wang [*a], Jingwen Yu[a], Xiaotong Meng[a], Pengfei Qiao[a] , Huabing Yin[b], Yongzhe Zhang[c] and Pu Wang[a]

Breast cancer is a type of heterogeneous disease which manifests as different molecular subtypes due to the complex nature of tumour initiation, progression, and metastasis. Accurate idenfication of a breast cancer subtype plays crucial roles for breast cancer management. Herein, taking the advantages of efficient quenching properties of black phosphorus nanosheets (BPNSs), in combination with the high specificity of ssDNA (or RNA) aptamer, a fluorometric duplexed assay that is capable of simultaneous detection of two tumour markers within one run is developed. When mixed with BPNSs, the fluorescence of both FAM and Cy3 labelled aptamers was quenched. The presence of different subtypes of breast cancer cells restored the FAM and Cy3 fluoresecence at distinct pattern according to their intrisic features. The proposed assay can precisely recognise label-free breast cancer subtypes, providing an efficient way for cell type identification and guidance for subsequent breast cancer treatment. The significance of the proposed study is two-fold. First we provide a simple way for sensitive and specific tumour cell detection; secondly, the proposed dual assay allows precise recognization of tumour cells and thus opens a door for rapid characterization and sorting of a wide range of tumours without using expensive instruments.

Introduction

Breast cancer is the most commonly occurring cancer in women, comprising almost one third of all malignancies in females. Breast cancer is not just a single type of disease, but rather a variety of intricate subtypes which require different treatment strategies.[1, 2] For instance, some breast cancers grow in response to hormone stimuli while others not. These different subtypes could be characterized by their genetic profiles. Precise recognition of a breast cancer subtype could potentially allow more effective personalized treatment and plays vital roles for improving the cancer management.

Nanomaterials have emerged as an effective stage for detecting biomedical molecules (DNA, peptide, glucose, cancer biomarkers etc.) or live pathological cells via various techniques.[3-5] Fluorescent nanomaterials, such as quantum dots (Qdots) and fluorescent carbon nanoparticles etc., are especially prominent for detection in biomedical applications due to the high sensitivity and reproducibility. Rather than acting as a fluorophore, some nanomaterial-based probes have been exploited by using nanomaterials as fluorescent quenchers. For instance, gold nanoparticles (AuNPs) have been described as highly efficient nanoquenchers. Functionalized with specially designed hair-pin structured aptamers, AuNPs were able to sense tumour-related proteins at high sensitivity.[6] Graphene Oxide (GO) and transition metal dichalcogenides (TMDs, including MoS2, WS2 etc.) were reported as nanoquenchers via long-range energy transfer and related nanoprobes have been successfully developed via coupling with biomolecular recognition events for the fluorometric detection of nucleic acids,[7, 8] proteins,[9] prostate cancer antigen (PSA),[10] metal ions[11, 12] and small molecules.[8, 13-15] Despite of that, it was reported that AuNPs either adsorb DNA too tightly (e.g. >10–13 nm) or too weakly (e.g. 0-3 nm), binding induced disassociation has not been a popular signalling method.[16] Whereas for GO, the surface is quite heterogeneous, displaying both hydrophobic regions favourable for DNA adsorption and highly oxidized regions that repel DNA. Biosensors based on DNA and surface interaction can be further improved via exploring new materials, improving the quench-recovery response time, tuning the DNA-surface interactions etc. to achieve higher sensitivity, better specificity and faster response. It is in this context we initiated this study.

Recently, black phosphorus (BP) has received enormous attention as a new 2D material. Although being a graphene analogue, some properties of BP even outperform those of graphene.[17, 18]

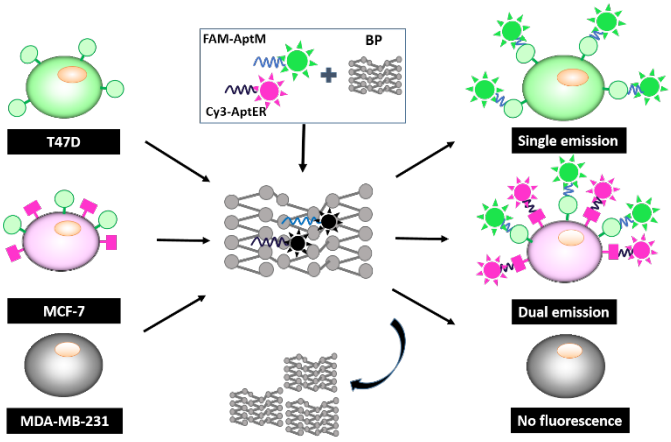

Scheme 1. A schematic illustration of the fluorometric switch for specific breast cancer cell recognition via fluorescent quench and restoration.

BP has a direct bandgap that is tuneable from 0.3 eV to 2.0 eV, which spans over the gap between graphene and 2D TMDs.[19] Moreover, the excellent charge-carrier mobility (up to 1000 $cm^2 \cdot V^{-1} \cdot s^{-1}$), good

[a] *Laboratory for Biomedical Photonics, Institute of Laser Engineering, Beijing University of Technology, Beijing, 100124, China.*
[b] *Biomedical Engineering Laboratory, School of Engineering, University of Glasgow, Oakfield Avenue, Glasgow G12 8LT, UK.*
[c] *College of Materials Science and Engineering, Beijing University of Technology, Beijing, 100124, China.*
†Electronic Supplementary Information (ESI) available: (1) Discussions of quenching mechanism of BP; (2) Quenching ability of BPNPs to Cy3-AptER; (3) Quenching ability of BPNPs to FAM-AptM.

current on/off ratio (ca. 10^4–10^5) and a striking in-plane anisotropy of BP render this 2D material a perfect candidate for nanoelectronics and nanophotonics.[20-23] BP nanomaterials also showed high biocompatibility and have been used in drug delivery, cancer therapy and photoacoustic imaging in biomedical area.[24-26] Nevertheless, applications of BP nanomaterials in label-free pathological cell sensing have not been explored.

Herein, we report that multi-layer black phosphorus nanosheets (BPNSs) functionalized with dual cell-recognizing aptamers can simultaneously and precisely recognize multiple subtypes of breast cancer cells. First, we demonstrate that BPNSs could quench the fluorescence of dye FAM. Subsequently we designed a probe via integrating BP and fluorescent aptamers. The proposed quench-and-recovery strategy is depicted in Scheme 1. Previously, the interaction of single strand DNA (ssDNA) with BP nanostructures has been examined experimentally.[27-29] BP multi-layer adsorbs dye-labelled ssDNA (or RNA) aptamer via van der Waals force between nucleobases and the basal plane of phosphorene, then quench the fluorescence of the dye. When the aptamer-BP complex is hybridized with target cells, the ssDNA aptamers recognize and interact with the cell, which disrupts the interaction previously formed between the ssDNA and multilayer BP. As a result, the dye-labelled probe is disassociated from BP, resulting in fluorescence restoration. Therefore, the fluorescence of the probe is expected to provide a quantitative readout of the target cell.

A single aptamer would only recognize one specific episode on the cell, which sometimes could result in false results. Integrating two or more specific aptamers onto BPNSs would overcome the shortcoming and allow precise recognition of dual cell surface markers in a single run with improved diagnostic specificity. This is important since one kind of tumour cell may express a variety of tumour markers.[30, 31] Such multi-aptamer approaches would take full advantage of the capabilities of a cell-based therapy, as cells usually integrate multiple inputs to modulate their natural decisions in sophisticated ways. Moreover, the simultaneous dual-analysis of cancer biomarkers can simplify the analytical procedure, enhance the detection throughput, and decrease the detection cost.

Results and discussion

Fabrication and Characterization

Bulk red phosphorus was transformed into micro-sized particles of BP via a high energy mechanical milling (HEMM) technique under ambient conditions.[32] BPNSs were fabricated from the micro-sized BP powder using a modified liquid exfoliation method. The as-exfoliated product was dispersed in ddH_2O. High resolution transmission electron microscopy (HRTEM) was employed to examine the morphology of as-exfoliated materials. Fig 1a shows a typical HRTEM image of the fabricated BP products, in which each individual nanostructure shows a planar morphology. Statistical analysis of HRTEM image indicated that most of the BPNSs were in an average size of 55±25 nm, see the inset of Fig 1a. As shown in Fig 1b, BPNSs have strong Raman-active stretching transitions at 362.52cm^{-1}, 439.33cm^{-1} and 466.59cm^{-1} which are attributed to A_g^1, B_{2g}, and A_g^2 vibrational modes.[18] Compared to bulk BP, the A_g^1, B_{2g}, and A_g^2 modes of BPNSs were blue-shifted by 0, 2.28, 1.13cm^{-1}, respectively. A similar blue shift has been observed for a few layers BPNSs and BP nanodots.[33] Raman signals of layered BP were less intensified compared to the bulk BP, which is in agreement with previous reports.[34] In an effort to elucidate the height of BPNSs, atomic force microscopy (AFM) imaging was performed at multiple locations across the sample. Due to resolution limitation of AFM, only larger size sheets were chosen for height measurement. The AFM topographic images in Fig 1c and d indicated the average height of BPNSs was 8±4 nm, corresponding to ~16±8 layers of phosphorene.

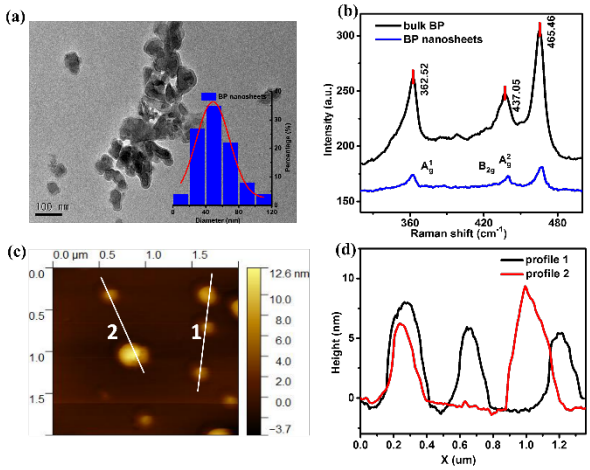

Fig 1. Topographic characterization of BPNSs: (a) HRTEM image of as-exfoliated products, inset shows the statistical results of 100 nanostructures; (b) Raman spectra of bulked BP (black line) and as-exfoliated BP nanostructures (blue line); (c) AFM image of a randomly selected region of an exfoliated sample;(d) Height distribution profile obtained from (c).

BPNSs quenched the fluorescence of FAM

Freshly prepared BPNSs were incubated with FAM. Fig 2a shows the fluorescence in the presence or absence of BPNSs, striking decreases of fluorescence intensities in the presence of BPNSs were observed. The quenching efficiency was positively correlated with the concentration of BPNSs (Fig 2b). To further investigate the long-term quenching by BPNSs, we evaluated the fluorescence in the presence of BPNSs for 24h. Immediate quench was observed for FAM. Maximum quench was quickly achieved and quenching efficiency remained unchanged for up to 24h (Fig 2c). Similarly, BPNSs also efficiently quenched the fluorescence of green fluorescent protein (GFP), Fig S1 (ESI†). The data clearly suggested that BPNSs had high quenching efficiency.

Assessment of the fluorescence lifetime (FLT) could provide strong evidence for identifying the quenching dynamics. The FLTs of FAM in the presence or absence of BPNSs were thus measured. As shown in Fig S2 (a) (ESI†), the FLTs of FAM in every case was almost synchronous, indicating the

quenching process by BPNSs was static quenching. The fitting of Stern-Volmer plot also indicates the involvement of static quenching. (For more details please refer to ESI). This is different from the data of a just accepted manuscript,[35] where both static and dynamic processes in the quenching of CsPbBr3 QD photoluminescence by FLBP were demonstrated.

When the FAM fluorescent emission peak was decreased, the photoluminescence emission of BPNSs (at 690 nm) was not intensified, suggesting that the quenching mechanism by BPNSs was not via non-radiative energy transfer, since a non-radiative energy transfer process is often featured by decreased donor emission with an associated increase of acceptor emission. Most likely, the high efficient quenching occurred through the light induced electron transfer from the photoexcited FAM to BPNSs.[32] BPNSs have very strong adsorption capacity, can adsorb molecules on its surface via ionic bond, dispersion force, van der Waals force etc.[29, 36, 37] Moreover, large surface area provides a better platform for adsorption, which would allow the fluorophores to form complexes with BPNSs, hence reduced the population of active, excitable fluorophores, resulted in high quenching capability of BPNSs.

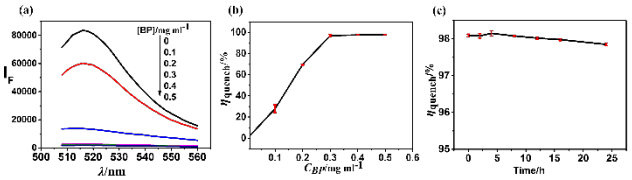

Fig 2. Quenching ability of BPNSs. (a) Fluorescence spectra of FAM in the presence of different concentrations of BPNSs as indicated; (b) Quenching efficiency for FAM is positively correlated with BP concentration. (c) Stable quenching by BPNSs over time. C_{FAM} =50fM, λex=470nm.

Sensing intracellular estrogen receptor (ER) of breast cancer cells

Breast cancers can be subtyped based on their molecular features, for instance hormone receptor positive (estrogen receptor positive (ER+) or progesterone receptor positive (PR+)), Her2-positive (Her2+), or triple negative (ER-, PR- and Her2-). Diagnosing the type of breast cancer is important for choosing the treatment approach since some medication is only efficient for one of these types. Approximately 70% of breast tumours are over expressing ER, referred to as ER+, and tumour cell proliferation is thought to be dependent on the activity of this hormone-mediated factor.

Equipped with the quenching property of BPNSs, we were in a very good position to design nanoprobes for bio-sensing. We first explored to probe ER+ breast cancer cells using BPNSs platform functionalized with Cy3-AptER, a fluorescently labelled RNA aptamer, which can specifically recognize intracellular ER. Since the side chains of RNA would have strong interaction with BPNSs, as illustrated in scheme 1, BPNSs efficiently quenched the fluorescence of Cy3-AptER in a dose-dependent manner (Fig S3 (ESI†)).

Then we examined a panel of breast cancer cells, including MCF7, T47D and MDA-MB-231, for their ability to restore the fluorescence. We chose a BP concentration which can quench 90% of Cy3-AptER fluorescence (Fig 3a black line) as a start point for the following assays. As shown in Fig 3a and b, the presence of MCF7 cells markedly restored the fluorescence of Cy3. The restored fluorescence was positively dependent on the cell number (Fig 3b). Maximum recovery was achieved with 10000 cells, by which 97.36% fluorescence was restored (Restoration ratio was calculated by equation $\eta_R=F_R/F_0$, where F_R and F_0 are the fluorescence intensities in the presence of cells and pure Cy3-AptER, respectively), indicating the binding between AptER and ER receptor reached saturation. When cell number went down to as low as 250, around 63.17% of fluorescence was restored. Cell number lower than 250 failed to restore the fluorescence. The response time of the probe was very fast. Immediate fluorescence restoration was observed uopn addition of the probe. In order to obtain more reliable and reproducible data, the target cells were incubated with the probe for 30-120min before measuring.

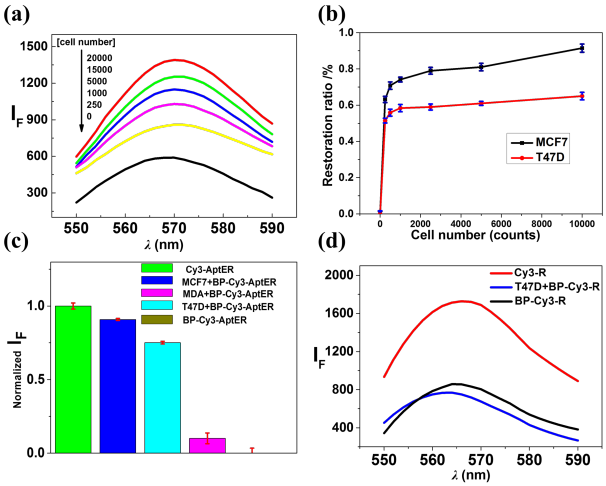

Fig 3. Fluorescence restoration by ER+ cells. (a) Fluorescence recovery in the presence of different numbers of MCF7 cells as indicated; (b) The dose-dependent relationship between MCF7, T47D cell number and recovered fluorescence; (c) Normalized recovered fluorescence intensity of Cy3 in different type of cells (cell number=10000). $C_{Cy3\text{-}AptER}$=100nM, C_{BP}=0.4mg/mL, λ_{ex}=500nm. (d) T47D cells failed to recover the quenched fluorescence of Cy3 labelled on a random sequence DNA (Cy3-R, 100nM).

Similar to MCF7, T47D breast cancer cells also efficiently restored the fluorescence (Fig 3b red line and 3c aqua bar), the maximum restoration was around 75.1% with a cell number of 10000. The higher maximum fluorescence recovered by MCF7 than T47D indicated the quantity of ER receptor in MCF7 cells was higher than that of T47D. Whereas MDA-MB-231 cells only restored 10% of the fluorescence with 10000 cells, which is much lower compared with MCF7 and T47D cells. The results were in good consistence with the published data that MCF7 and T47D cells are ER+, while MDA-MB-231 cells are ER negative. A random RNA sequence labelled with Cy3 (Cy3-R)

was tested in parallel. The fluorescence of Cy3-R was also quenched efficiently by BPNSs (Fig 3d. black line); however, the fluorescence was not restored by either MCF7 or T47D cells (Fig 3d, blue line), indicating the specificity of AptER

.

In our experiments, we observed excellent fluorescence restoration in the presence of target cells, indicating that both the function and specific secondary structure of AptER were well retained upon interaction with BPNSs.

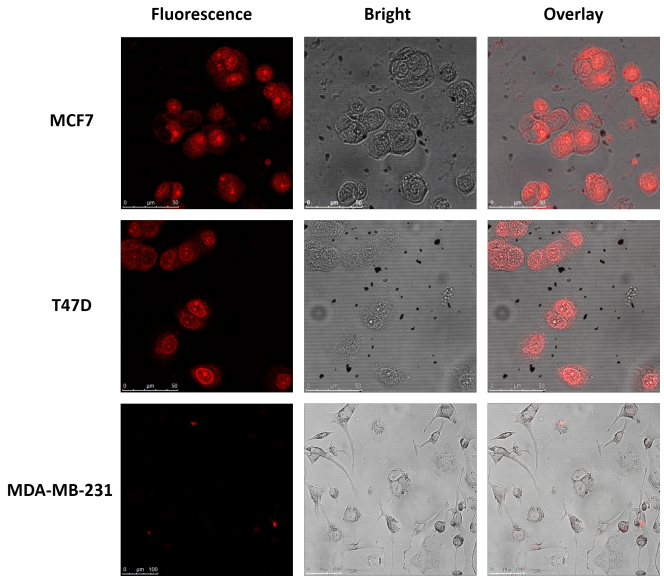

Fig 4. LSCM images of BPNSs/Cy3-AptER treated cells. Cells were incubated with BPNSs/Cy3-AptER nanoconstructs for 2h, then washed with PBS and imaged by LSCM. Cell number = 10000, $C_{Cy3\text{-}AptER}$=100nM, C_{BP}=0.4mg/mL，λex=514nm.

To confirm the results obtained from the spectrofluorometer, laser scanning confocal microscopic (LSCM) analysis was performed to further elucidate the aptamer-cell interaction and fluorescence recovery. As shown in Fig 4, after treated with BPNSs/Cy3-AptER complex, the majority of MCF7 cells were stained with Cy3, the nuclei were particularly heavily stained since ERs were more recognized as a nuclear receptor. T47D cells were stained both on the cell membrane and in the nuclei. Whereas few MDA-MB-231 cells were stained. The imaging results were in good consistence with the fluorometric data.

Sensing cell surface marker MUC1

Similar to the experiment above, we replaced the Cy3-AptER aptamer with FAM-AptM, a FAM labelled ssDNA aptamer that can recognize a specific surface marker MUC1 of MCF7 cells. The fluorescence of FAM-AptM was efficiently quenched by BPNSs in a dose dependent manner (Fig S4 (ESI†)).

In the presence of different numbers of MCF7 cells (0, 100, 250, 500, 1000, 2500, 5000, 8000, 10000, 15000, 20000), a striking cell number-dependent restoration of the FAM fluorescence was observed (Fig 5a, b). Maximum recovery was achieved with 15000 cells, the recovery rate was 106.67% (Fig 5b). In the range of 0-2000 cells, there was a linear relationship, as shown in figure 5b inset. The limit of detection (LOD) was calculated to be 65 cells according to the fitting curve based on an S/N ratio of 3, which is lower than the LOD of an AuNPs-based assay platform whose LOD was 81 cells.[38] The fluorescence of a random sequenced ssDNA labelled with FAM (FAM-R) was also quenched by BPNSs (Fig 5c black line); however, it was not restored by MCF7 cells (Fig 5c, blue line). The shape of the saturation curve of AptM/MUC1 (Fig 5b) binding was different from that of AptER/ER (Fig 3b) binding, suggesting the dissociation constants (Kd) were different. The capabilities of three types of breast cancer cell to restore the fluorescence of FAM were compared as shown in Fig 5d. Clearly, only MCF7 cells completely restored the fluorescence to the level of pure FAM-AptM (blue bar in Fig 5d);

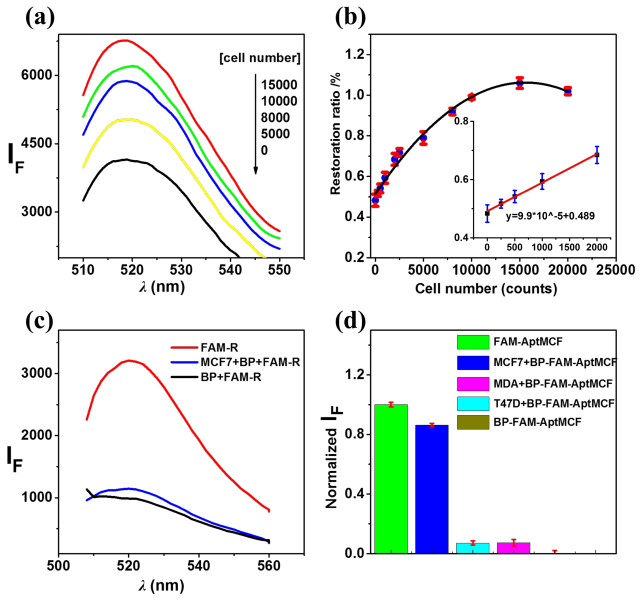

Fig 5. MCF7 cells efficiently restored the fluorescence. (a) Fluorescence recovery in the presence of different numbers of MCF7 cells as indicated; (b) The calibration curve of linear relationship between MCF7 cell number and recovered fluorescence intensity; (c) MCF7 cells failed to recover the fluorescence of FAM labelled on a random sequence DNA (FAM-R, 50nM); (d) Normalized fluorescence recovery of FAM by different type of cells (cell number=10000).$C_{FAM\text{-}AptM}$=50nM, C_{BP}=0.25mg/mL, λex=470nm.

while T47D (aqua bar) and MDA-MB-231 (purple bar) cells failed to restore the fluorescence. This clearly indicated the high specificity of the aptamer toward MCF7 cells. To confirm the results, MCF7 cells were incubated with BPNSs/FAM-AptM complex for 2h and imaged using LSCM. Most MCF7 cells were stained with FAM-AptM on the cell surface (Fig 6), which is consistent with the fact that AptM aptamer is a specific surface marker of MCF7 cell. In contrast, neither T47D nor MDA-MB-

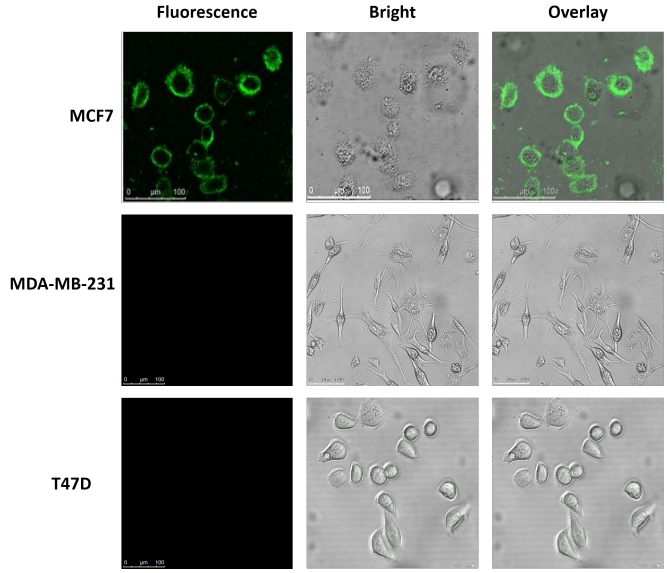

231 cells were stained with FAM-AptM, which was consistent with the spectrofluorometric data.

Fig 6. LSCM images of BPNSs-FAM-AptM treated cells. Cells were incubated with BPNSs-FAM-AptM nanoconstructs for 2h, then washed with PBS and imaged by LSCM. Cell number = 10000, $C_{FAM\text{-}AptM}$=50nM, C_{BP}=0.25mg/mL，λex=488nm.

The sensing parameters of our assay and published data in the area of tumour cell detection using fluorescence off-on switch were summarized in Table 1. The selectivity, detection limit and response time of our proposed sensing platform were ranked on the top.

Precise and simultaneous recognition of multiple types of breast cancer cells

Attempting to discriminate breast cancer cells via a single aptamer/BPNSs approach that only recognizes a single cell surface marker is intrinsically a one-dimensional approach, and it will not encounter the need of precise detection. As showed above, BPNSs/Cy3-AptER nanoconstruct not only recognized MCF7 cells, also recognized T47D cells. In addition, probes with single recognising event is often related with false-positive results, to some extent, due to low specificity of a aptamer. It would be a significant improvement if multiple aptamers could be used to combinatorially detect multiple cell surface characters since one kind of tumour cell may express a variety of tumour markers.[30, 31] Such multi-aptamer approaches would take full advantage of the capabilities of a cell-based therapy, as cells usually integrate multiple inputs to modulate their natural decisions in sophisticated ways.

To this end, we investigated dual aptamer-BPNSs nanoconstruct for precise recognition. 100nM Cy3-AptER and 50nM FAM-AptM were mixed with 0.4 mg/mL of BPNSs in one-pot as illustrated in scheme 1. At these concentrations, BPNSs quenched >90% of the fluorescence of both Cy3 and FAM. The resulted mixture showed very low level of Cy3 and FAM emission (Fig 7a, black lines). The mixture was incubated with a panel of breast cancer cells including MCF7, T47D and MDA-MB-231, respectively. Following incubation for 2h, fluorescence was measured. MCF7 cells showed dual fluorescent emission at 520nm and 570nm (Fig 7a, aqua lines), indicating simultaneous dual restoration of FAM and Cy3. In the case of T47D cells (Fig 7a, green lines), 68.7% of Cy3 fluorescence was recovered while FAM fluorescence was hardly restored. Whereas for MDA-MB-231 cells (Fig 7a, purple lines), neither FAM nor Cy3 fluorescence was restored. The dual sensing results were plotted in a heat map as shown in Fig 7(b). Obviously, three types of breast cancer showed distinct readouts from the duplexed assay. The assay results provided valuable information in discriminating different type of cells.

The most precisely identified cell line via this assay was MCF7. MCF7 is a widely studied *in vitro* model for breast cancer. The MCF7 cell line has functional estrogen receptors (ER) and is dependent on estrogen for growth. Thus, onset and progression of human breast cancer is dependent upon ovarian estrogens. For this type of cancer, hormone treatment, e.g. anti-estrogen treatment (drug tamoxifen and benzothiophene), would result in high treatment efficiency. Clearly, accurate identification of MCF7 cells would provide vital guidance for the subsequent therapy. T47D cells were identified as ER+, which is consistent with published data. It would be more accurate if the assay could incorporate another T47D-specific aptamer to further confirm the molecular trait of T47D.

In this assay, we used well characterized subtypes of breast cancer cells, the resulted data were in good consistence with

Table 1. comparison of sensing parameters of various methods

Materials	Probe	Target episode	Target cells	LOD	Linear range	Response time	ref
BPNS	Aptamer	MUC1 ER	MCF7 MCF7, T47D	65cells	0-2000cells	0-30min	
AuNP	Aptamer	MUC1	MCF7	81cells	200-12000cells	180min	38
GO/AuNWs	sDNA	miRNA-21	MCF7	NA	NA	14h	39
GO-based	Aptamer	PTK	CCRF-CEM	25cells mL^{-1}	25-25000cells mL^{-1}	20min	40
GO	Aptamer	cell	SMMC-7721	200cells	NA	30min	41
GO	Aptamer Sgc8	cell	CCRF-CEM	10cells	100-1×10^{7}cells	30min	42
sDNA	Aptamer	MUC1	A549	10cells mL^{-1}	10-1000cells mL^{-1}	45min	43

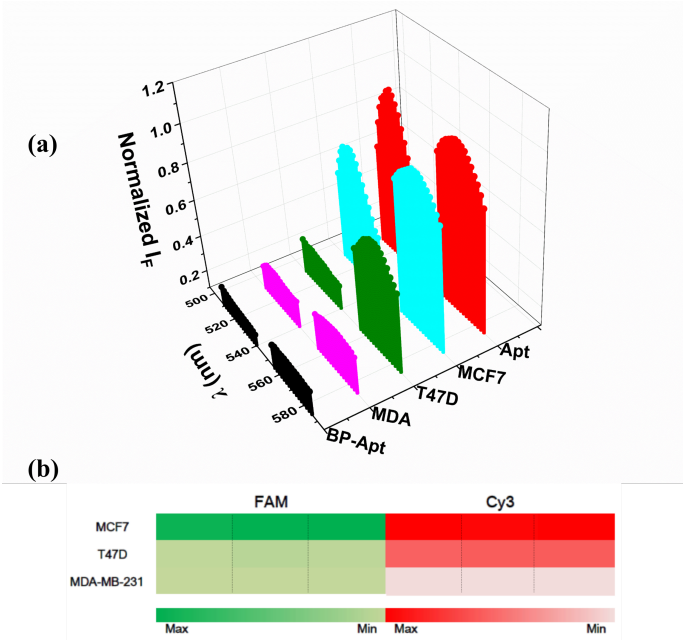

Fig 7. Duplexed assay of breast cancer cell discrimination via BPNSs-Aptamers nanoconstruct. (a) BPNSs/FAM-AptM/Cy3-AptER nanoconstruct was incubated with various cell lines (15000 cells each) for 2h, then fluorescence was measured. $C_{FAM\text{-}AptM}$=50nM, $C_{Cy3\text{-}AptER}$=100nM, C_{BP}=0.4mg/mL, $\lambda_{ex\text{-}FAM}$=488nm, $\lambda_{ex\text{-}Cy3}$=500nm. (b) Heat map showing the differential expression of dual tumour markers in various breast cancer cell lines shown as FAM and Cy3 intensity, respectively. the distinguishing features of the tested cell lines, indicating the proposed assay is reliable for cell identification.

Conclusions

In summary, with an aim to better characterize breast cancer subtypes in a quick, sensitive, and quantitative way, we have developed a duplexed assay that is capable of simultaneously label-free detection of two tumour markers within one run. Our proposed assay involved the use of an efficient nanoquencher (BPNSs) and two fluorescently labelled aptamers with specific recognition. We demonstrated that our setup was capable of precisely discriminating three breast cancer subtypes. Currently, the most commonly used technique for cell-based analysis is flow cytometry. It is expensive and requires large number of cells, tedious sample preparation and complex data analysis. Our proposed setup can be measured as a facile and cost-effective alternative for quick pre-screen of cells. Such setup offered distinct benefits: (i) multiplexed biomarker detection could be achieved via incorporating multiple specific aptamers in the setup. Nevertheless, it is worth noting that, due to the broad emission of a fluorescent dye that may result in spectral overlap, fluorophores used for labelling should be carefully selected. (ii) easy interpretation of detection outcomes without the need for further data processing; (iii) applicable to clinical samples such as tissue biopsy specimens and blood samples. The combination of BPNSs and aptamers shows great potential as a cancer screening platform for multiplexed tumour cell subtyping. In addition, the large surface area and high bio-compatibility of BPNSs make this material an excellent aptamer carrier for the assay.

The implementation of the current work would lay important foundation for future applications, especially in the field of circulating tumour cell capturing and simultaneous detection. The non-fluorescent BPNSs-Aptamers complex can be immobilized to a microfluidic device, for instance, microfluidic chips or micro-structured optical fibres, to achieve capturing and identification of tumour cells simultaneously. Besides the detection of tumour cells, the proposed assay could be readily adopted for the multiple detection of other oncogenic biomarkers such as RNA, DNA, single nucleotide variants (SNVs) or DNA methylation by changing the aptamer sequences. Although, in this assay, well-characterized breast cancer cells were used, it holds great potential in clinic to identify unknown type of cells with distinct character. Hence, we believe the present demonstration and promise of our proposed assay hold great potential for breast cancer cell subtyping and personalized therapy.

Experimental

Materials and reagents

The fluorescent aptamers FAM-AptM (5'-GGC TAT AGC ACA TGG GTA AAA CGA C-FAM), ^{48}Cy3-AptER (Cy3-GGG GUC AAG GUG ACC CC-3'),[49] Cy3-R (Cy3-AUCGUGUGCUGCUACGA-3') and FAM-R (5'-TCA AAG CAT TCA GTC GAG AT-FAM) were purchased from Beijing Sunbiotech Co. Ltd (Beijing, China). All Materials and reagents were of biotechnology grade and used without further purification. Ultrapure water with an electrical resistance 18 MΩ cm-1 was used in all the experiments.

Preparation and characterization of BPNSs

BPNSs preparation details and TEM, AFM, Raman details. The BPNSs were prepared using the liquid exfoliation technique. Particularly, 20 mg of the BP powder was dispersed in 40 mL of ultrapure water. Then the mixture solution was sonicated in ice water with a sonic tip for 3h (On/Off cycle: 5s/2s, power: 300w, frequency: 20 KHz), followed by bath sonication for 5 hours (ddH2O) on ice. The ice water was utilized to keep a relatively low temperature of the system. Finally, the supernatant was collected after centrifuged the dark brown suspension at 5000 rpm for 1.5h to remove the residual unexfoliated particles. Before use, the prepared BPNSs were sonicated in ice water with a sonic tip for 5min (On/Off cycle: 5s/2s, power: 300w, frequency: 20 KHz) to avoid reunion. The morphology and size of as-prepared BPNSs were characterized with a JEM-2100 transmission electron microscopy (TEM) at 200 kV on a carbon-coated copper grid and an atom force microscopy (AFM) (MI, USA). The horizontal size and height distributions of BPNSs were estimated based on statistical analysis TEM and AFM images by Nanomeasurer 1.2. Raman spectra of BPNSs was performed on a high-resolution confocal Raman microscope at room temperature.

Cell culturing

Breast cancer cell lines MCF7, MDA-MB-231 and T47D were purchased from the American Type Culture Collection (ATCC).

All cell lines were cultured in a DMEM medium (Thermo Scientific) with 10% FBS, 1% penicillin and 1% streptomycin in an incubator with 5% CO2 and 88% humidity at 37 °C. Healthy, stable cells in logarithmic growth phase were used for all experiments. To count the number of cells, we use CountessTM automated cell counter (Invitrogen, Korea).

Fluorescent measurement

FAM-AptM (final concentration 50nM) was mixed with different concentrations BP nanoquencher ranging from 0 to 0.35mg/ml. PBS solution was supplemented to make the final solution volume to be 100μL. Then, fluorescent intensity was measured on a spectrophotometer (Berthold Technologies GmbH & Co.KG, Germany) with the excitation of 470 nm. For cell detection, BPNSs was mixed with FAM-AptM for 5mins (BP-FAM-AptM, CBP=0.25 mg/mL, CFAM-AptM=50nM) and then BP-FAM-AptM was incubated with an increasing count of target cells (2500, 5000, 8000, 10000, 15000, 20000) for 2h in dark. After rinsing with PBS buffer for twice, the fluorescence intensity was measured. All the fluorescence intensities were recorded using the same method.

Laser scanning confocal microscope (LSCM) analysis

Breast cancer cell lines were cultured in 96-well plate with 1×104 per well to adhere for 6h. Then added the BP-FAM-AptM mixture (CBP=0.25mg/mL, CFAM-AptM=50nM, reaction fully) to MCF7 cells for 2h. After rinsing with PBS buffer, the 96-well plate was mosaicked and images of the samples were acquired at 488 nm light excitation on a laser scanning confocal platform (Leica TCS SP8). The LSCM data were processed with the Leica Application Suite AF software.

Time-resolved fluorescence measurement (lifetime determination)

Lifetime was measured and fitted by a fluorescence lifetime imaging microscope. Manufactured based on Olympus FV1200 and PicoQuant LSM upgrade Kit. 488nm pulsed laser was used to excite the fluorescence of BP-FAM, the repetition frequency was 40MHz and the output power was 264.1 nW. The signal was collected within the range of 500-560 nm.

Statistical Analyses

Each experiment was repeated three times. The data were processed using the Origin9.0 software. Data were presented as Mean ± SD.

Conflicts of interest

There are no conflicts to declare.

Acknowledgements

Funding of this research was supported by the National Natural Science Foundation of China. (No: 61378088), fund for Biophotonics Innovative Personnel Base Construction (BIPB101000541212011) and fund for Advanced Manufacturing Technology (AMF101000541213504) by Beijing University of Technology. We thank Yanli Zhang from Tsinghua University for help in optical techniques.

Notes and references

1 J. S. de Bono A. Ashworth. *Nature,* 2010, **467***,* 543-549.

2 F. S. Collins H. Varmus. *New England Journal of Medicine,* 2015, **372***,* 793-795.

3 Y. Khan, A. R. Li, L. Chang, L. D. Li L. Guo. *Sensors and Actuators B-Chemical,* 2018, **255***,* 1298-1307.

4 Q. Yao, F. Cao, M. Lang, C. Feng, X. Meng, Y. Zhang, Y. Zhao X.-h. Wang. *Journal of Materials Chemistry B,* 2017, **5***,* 5165-5175.

5 S. D. Zhang, R. Geryak, J. Geldmeier, S. Kim V. V. Tsukruk. *Chemical Reviews,* 2017, **117***,* 12942-13038.

6 S. Hamd-Ghadareh, A. Salimi, F. Fathi S. Bahrami. *Biosensors & Bioelectronics,* 2017, **96***,* 308-316.

7 J. Balapanuru, J. X. Yang, S. Xiao, Q. Bao, M. Jahan, L. Polavarapu, J. Wei, Q. H. Xu K. P. Loh. *Angew Chem Int Ed Engl,* 2010, **49***,* 6549-53.

8 C. Zhu, Z. Zeng, H. Li, F. Li, C. Fan H. Zhang. *J Am Chem Soc,* 2013, **135***,* 5998-6001.

9 S. Gan, L. Zhong, D. Han, L. Niu Q. Chi. *Small,* 2015, **11***,* 5814-25.

10 Y. Ueno, K. Furukawa, A. Tin H. Hibino. *Analytical Sciences,* 2015, **31***,* 875-879.

11 Y. Q. Wen, C. Peng, D. Li, L. Zhuo, S. J. He, L. H. Wang, Q. Huang, Q. H. Xu C. H. Fan. *Chemical Communications,* 2011, **47***,* 6278-6280.

12 Y. Q. Wen, F. F. Xing, S. J. He, S. P. Song, L. H. Wang, Y. T. Long, D. Li C. H. Fan. *Chemical Communications,* 2010, **46***,* 2596-2598.

13 C. H. Lu, H. H. Yang, C. L. Zhu, X. Chen G. N. Chen. *Angew Chem Int Ed Engl,* 2009, **48***,* 4785-7.

14 S. He, B. Song, D. Li, C. Zhu, W. Qi, Y. Wen, L. Wang, S. Song, H. Fang C. Fan. *Advanced Functional Materials,* 2010, **20***,* 453-459.

15 W. Qiang, H. Hu, L. Sun, H. Li D. Xu. *Anal Chem,* 2015, **87***,* 12190-6.

16 W. J. Wang, C. L. Chen, M. X. Qian X. S. Zhao. *Analytical Biochemistry,* 2008, **373***,* 213-219.

17 Y. Zhao, Y. Chen, Y.-H. Zhang S.-F. Liu. *Materials Chemistry and Physics,* 2017, **189***,* 215-229.

18 Z. Sofer, D. Bousa, J. Luxa, V. Mazanek M. Pumera. *Chem Commun (Camb),* 2016, **52***,* 1563-6.

19 V. Eswaraiah, Q. Zeng, Y. Long Z. Liu. *Small,* 2016, **12***,* 3480-502.

20 H. Liu, A. T. Neal, Z. Zhu, Z. Luo, X. F. Xu, D. Tomanek P. D. Ye. *Acs Nano,* 2014, **8***,* 4033-4041.

21 R. Roldan A. Castellanos-Gomez. *Nature Photonics,* 2017, **11***,* 407-409.

22 P. He, J. R. Brent, H. Ding, J. Yang, D. J. Lewis, P. O'Brien B. Derby. *Nanoscale,* 2018, **10***,* 5599-5606.

23 A. Castellanos-Gomez. *Journal of Physical Chemistry Letters,* 2015, **6***,* 4873-4873.

24 Z. Sun, Y. Zhao, Z. Li, H. Cui, Y. Zhou, W. Li, W. Tao, H. Zhang, H. Wang, P. K. Chu X. F. Yu. *Small,* 2017, **13***,* 1602896

25 H. U. Lee, S. Y. Park, S. C. Lee, S. Choi, S. Seo, H. Kim, J. Won, K. Choi, K. S. Kang, H. G. Park, H. S. Kim, H. R. An, K. H. Jeong, Y. C. Lee J. Lee. *Small,* 2016, **12***,* 214-9.

26 C. Sun, L. Wen, J. Zeng, Y. Wang, Q. Sun, L. Deng, C. Zhao Z. Li. *Biomaterials,* 2016, **91***,* 81-89.

27 N. Varghese, U. Mogera, A. Govindaraj, A. Das, P. K. Maiti, A. K. Sood C. N. Rao. *Chemphyschem,* 2009, **10***,* 206-10.

28 P. Hobza. *Phys Chem Chem Phys,* 2008, **10***,* 2581-3.

29 Y. T. Yew, Z. Sofer, C. C. Mayorga-Martinez M. Pumera. *Materials Chemistry Frontiers,* 2017, **1***,* 1130-1136.

30 K. T. Roybal, L. J. Rupp, L. Morsut, W. J. Walker, K. A. McNally, J. S. Park W. A. Lim. *Cell,* 2016, **164***,* 770-779.

31 D. M. Barrett, D. T. Teachey S. A. Grupp. *Current Opinion in Pediatrics,* 2014, **26***,* 43-49.

32 C. M. Park H. J. Sohn. *Advanced Materials,* 2007, **19***,* 2465.

33 L. Cartz, S. R. Srinivasa, R. J. Riedner, J. D. Jorgensen T. G. Worlton. *Journal of Chemical Physics,* 1979, **71***,* 1718-1721.

34 C. A. Vanderborgh D. Schiferl. *Physical Review B,* 1989, **40***,* 9595-9599.

35 Subas Muduli, Padmini Pandey, Gayathri Devatha, Rohit Babar, Thripuranthaka M, D. C., Kothari, Mukul Kabir, Pramod Pillai, Satishchandra Ogale. Angew. Int. Ed. 10.1002/anie.201712608.

36 W. S. Chen, J. Ouyang, H. Liu, M. Chen, K. Zeng, J. P. Sheng, Z. J. Liu, Y. J. Han, L. Q. Wang, J. Li, L. Deng, Y. N. Liu S. J. Guo. *Advanced Materials,* 2017, **29***,* 1603864.

37 W. Zhang, T. Huynh, P. Xiu, B. Zhou, C. Ye, B. Luan R. Zhou. *Carbon,* 2015, **94***,* 895-902.

38 B. Yang, B. B. Chen, M. He, X. Yin, C. Xu B. Hu. *Analytical Chemistry,* 2018, **90***,* 2355-2361.

39 Y. X. Piao, F. Liu T. S. Seo. *Acs Applied Materials & Interfaces,* 2012, **4***,* 6784-6788.

40 X. Y. Sun, P. C. Liu, L. L. Wu B. Liu. *Analyst,* 2015, **140***,* 6742-6747.

41 B. E. F. de Avila, A. Martin, F. Soto, M. A. Lopez-Ramirez, S. Campuzano, G. M. Vasquez-Machado, W. W. Gao, L. F. Zhang J. Wang. *Acs Nano,* 2015, **9***,* 6756-6764.

42 L. L. Cao, L. W. Cheng, Z. Y. Zhang, Y. Wang, X. X. Zhang, H. Chen, B. H. Liu, S. Zhang J. L. Kong. *Lab on a Chip,* 2012, **12***,* 4864-4869.

43 Y. Wang, Z. H. Li, T. J. Weber, D. H. Hu, C. T. Lin, J. H. Li Y. H. Lin. *Analytical Chemistry,* 2013, **85***,* 6775-6782.

44 J. Ju, R. Z. Zhang, S. J. He W. Chen. *Rsc Advances,* 2014, **4***,* 52583-52589.

45 D. D. Yang, M. Liu, J. Xu, C. Yang, X. X. Wang, Y. B. Lou, N. Y. He Z. F. Wang. *Talanta,* 2018, **185***,* 113-117.

46 S. R. Ryoo, J. Lee, J. Yeo, H. K. Na, Y. K. Kim, H. Jang, J. H. Lee, S. W. Han, Y. Lee, V. N. Kim D. H. Min. *Acs Nano,* 2013, **7***,* 5882-5891.

47 Q. Xie, Y. Y. Tan, Q. P. Guo, K. M. Wang, B. Y. Yuan, J. Wan X. Y. Zhao. *Analytical Methods,* 2014, **6***,* 6809-6814.

48 C. S. M. Ferreira, M. C. Cheung, S. Missailidis, S. Bisland J. Gariepy. *Nucleic Acids Research,* 2009, **37***,* 866-876.

49 R. Ahirwar, S. Nahar, S. Aggarwal, S. Ramachandran, S. Maiti P. Nahar. *Scientific Reports,* 2016, **6***,* 21285.